Advances in Geo-Energy Research

Vol. 7, No. 1, p. 7-19, 2023

Original article

# Comparative study on the thermal performance and economic efficiency of vertical and horizontal ground heat exchangers

Qiliang Cui[1], Yu Shi[1]*, Yulong Zhang[1], Rui Wu[2], Yifan Jiao[1]

[1]*Faculty of Geosciences and Environmental Engineering, Southwest Jiaotong University, Chengdu 611756, P. R. China*

[2]*Department of Earth Sciences, ETH Zürich, Zurich 8092, Switzerland*

**Keywords:**
Geothermal energy
ground heat exchanger
comparative study
thermal performance
economic efficiency

**Cited as:**
Cui, Q., Shi, Y., Zhang, Y., Wu, R., Jiao, Y. Comparative study on the thermal performance and economic efficiency of vertical and horizontal ground heat exchangers. Advances in Geo-Energy Research, 2023, 7(1): 7-19.
https://doi.org/10.46690/ager.2023.01.02

**Abstract:**
The ground-coupled heat pump is a shallow geothermal exploitation method taking soil as the thermal energy source. The ground heat exchanger is an important component of this system, which includes vertical or horizontal configurations. However, to the best of our knowledge, few studies exist involving the comparison of thermal performances and installation costs of two heat exchanger types considering the influence of ground climate, which makes the selection of heat exchanger configuration challenging for a specific field application. Hence, a 3-dimensional numerical model considering the variations of atmospheric conditions and soil water content is constructed in this paper. Based on this model, the thermal performances and economical efficiencies of vertical and horizontal ground heat exchangers are compared. The results indicate that the thermal performance difference between the two heat exchangers is greater in winter than in summer. The thermal performance is hardly influenced by the injection mass flow rate, while it is considerably affected by the length of heat exchanger. The thermal power rises linearly with the increase in heat exchanger length, and the increment of the vertical ground heat exchanger is higher. In addition, when the heat exchanger length is shorter than 40 m, the installation cost and thereby the total cost of the horizontal ground heat exchanger is considerably higher. With regard to both the thermal performance and economic efficiency, a vertical ground heat exchanger is only recommended when installing a single shallow ground heat exchanger.

## 1. Introduction

As the world's largest energy producer and consumer, China is developing clean, carbon-free and efficient new energy sources to achieve the goal of carbon neutralization and promote a harmonious relationship between humans and nature. Geothermal energy is one of the most important renewable energy resources because of its great exploitation potential and abundant reserves (Kazemi and Ehyaei, 2018; Chen et al., 2019). Therefore, paying attention to the rational development and utilization of geothermal resources is of great significance to realize the energy revolution.

Geothermal resources can be divided into three categories (Zhang and Hu, 2018): (1) convection, which is associated with recent volcanism or magmatic intrusion; (2) conduction, which is related to the deep circulation of groundwater; and (3) shallow geothermal energy (at a depth of less than 200 m). These resources could be utilized for power generation and as direct heat source, such as for bathing, room heating, aquaculture, etc. (Zhang and Hu, 2018; Muther et al., 2022). Shallow geothermal resources are the main focus of this paper, which are always exploited by the ground-coupled heat pump, taking soil as the thermal energy source. The common configurations of ground heat exchanger include the vertical ground heat exchanger (VGHE) and the horizontal ground heat exchanger (HGHE). In general, the HGHE is installed in areas without hard rocks, such as residential areas with large gardens. On the other hand, the VGHE is more appropriate in limited areas with complex rock distribution and hydrological environment, such as some small towns. Numerous studies

Yandy Scientific Press

*Corresponding author.
*E-mail address*: cuiqiliang1112@163.com (Q. Cui); shiyu@swjtu.edu.cn (Y. Shi); zyl20010622@163.com (Y. Zhang); rui.wu@erdw.ethz.ch (R. Wu); j247018642f@163.com (Y. Jiao).

Received June 1, 2022; revised July 1, 2022; accepted July 18, 2022; available online July 25, 2022.

have focused on ground heat exchangers. For VGHE, Gosselin et al. (2017) simulated the performance of single U, double U and coaxial ground heat exchanger pipes with high-density polyethylene and nanocomposite materials, and found that the performance of double U pipes with nanocomposite materials was superior to others. Javadi et al. (2019) proposed eight new helical ground heat exchangers and compared them with a single U-tube heat exchanger. Their study pointed out that the triple helix heat exchanger was better than the other configurations. Dada et al. (2016) simulated several case studies with different types of hot fluid carrier, and indicated that the effect of pure water as circulating fluid was better than that of ethylene glycol and gasoline. Kong et al. (2017) analyzed the thermal performance of a set of buried vertical U-tubes designed with different petals for ground-source heat pump and investigated different influential factors of thermal response. They found that the system performance increased gradually with the increase of inlet flow rate. These studies mainly focused on the heat exchangers and the fluid in the pipe without considering the effects of other factors around the heat exchangers. Previous studies for the VGHE have mainly considered the effects of groundwater flow, soil properties, operational parameters, and ground heat exchanger (GHE) structures on the thermal performance.

The soil temperature around the VGHE is relatively constant, but it is easily affected by the soil layers. Therefore, the HGHE is becoming increasingly popular in GHE studies. Kim et al. (2018) estimated the impacts of the geometry factor of spiral-coil on the thermal performance of a horizontal spiral-coil GHE, and pointed out that the coil center distance was the key factor affecting the performance, and the coil diameter had an ignorable effect on the heat exchange performance. Habibi and Hakkaki-Fard (2018) compared the techno-economic performances of four types of heat exchangers: linear, spiral, horizontal, and vertical slinky. The results demonstrated that the initial installation costs of spiral and linear heat exchangers in a single and parallel arrangement were the lowest. Pu et al. (2018) compared the performances of HGHE under in-line and staggered arrangement, and indicated that the performance of staggered arrangement was better. Tang and Nowamooz (2020) established a numerical model to simulate the interaction between surface environment and soil, and found that this interaction had a great impact on the heat exchanger performance. Yang et al. (2021) analyzed the effects of operation mode, groundwater seepage and long-term operation conditions on the HGHE. They discovered that under the annual operation conditions, intermittent operation was more conducive to the recovery of soil temperature, and the enhancement effect of groundwater seepage in the vertical direction was superior to that in the horizontal direction. Although the HGHE effectively overcomes certain shortcomings of the VGHE, it is seriously affected by surface radiation and precipitation due to its shallow installation depth.

Both kinds of heat exchangers have their own advantages and drawbacks. However, few comparative studies have focused on the thermal performances and economical efficiencies between VGHE and HGHE under the same tube length and environmental conditions. To this end, based on a fluid flow and heat transfer numerical model for the GHE considering atmosphere conditions and humidity migration, this paper comprehensively compares the thermal performances of VGHE and HGHE with the same tube length and environmental conditions. Moreover, the sensitivity and economic efficiency of these two heat exchangers are analyzed. The results are expected to provide the theoretical and scientific basis for the reasonable installation of shallow heat exchangers.

## 2. Model description

### 2.1 Mathematical model

#### 2.1.1 Atmosphere-HGHE-soil interaction

The two types of heat exchangers are installed in the shallow soil, and they are greatly affected by surface meteorological factors. The interactions between the atmosphere, GHE and soil are illustrated in Fig. 1. The water cycle between atmosphere and soil is a process of mass conservation and can be expressed as (Dietrich et al., 2016):

$$P = W_r + E + W_i \tag{1}$$

where $P$ denotes the precipitation, mm/s; $E$ denotes the evaporation, mm/s; $W_r$ and $W_i$ indicate respectively the water runoff and infiltration, mm/s. It is assumed that 10% of the precipitation runs off and the other evaporates or infiltrates into the ground. $E$ can be calculated by the following equation (Monteith, 1965; Chen and Buchberger, 2018; Tang and Nowamooz, 2020):

$$E = P\left[1 + \left(\frac{E_e}{P}\right)^{-2}\right]^{-\frac{1}{2}} \tag{2}$$

where $E_e$ denotes the evaporation potential, mm/s. This can be performed by the Penman-Monteith model, and the average air humidity is set as 0.80 in this paper (Monteith, 1965; Tang and Nowamooz, 2020).

The heat transfer between atmosphere and soil conforms to the energy conservation and can be expressed as (Chalhoub et al., 2017):

$$R_n + H - LE - G = 0 \tag{3}$$

where $H$ and $R_n$ represent respectively the sensible heat and the net radiation heat, W/m$^2$; $L$ represents the latent heat vaporization, J/kg, and the $L$ of water under the atmospheric pressure is 2.257 J/kg (Tang and Nowamooz, 2020); $G$ denotes the heat flux through the top of the heat exchanger, W/m$^2$.

The sensible heat flux $H$ is calculated by the difference between the ground surface and ambient temperature (Choi et al., 2018):

$$H = \rho_a c_{p,a} \frac{T_a - T_s}{r_a} \tag{4}$$

where $\rho_a$ denotes the air density, kg/m$^3$, and is set as 1.25 kg/m$^3$; $c_{p,a}$ denotes the air heat capacity, J/(kg·K), and is equal to 1003 J/(kg·K) (Tang and Nowamooz, 2020); $T_a$ and $T_s$ indicate the ground surface and ambient temperature, K; $r_a$ is the aerodynamic, s/m, and is set as 276.90 s/m here.

The net radiation heat $R_n$ is calculated by:

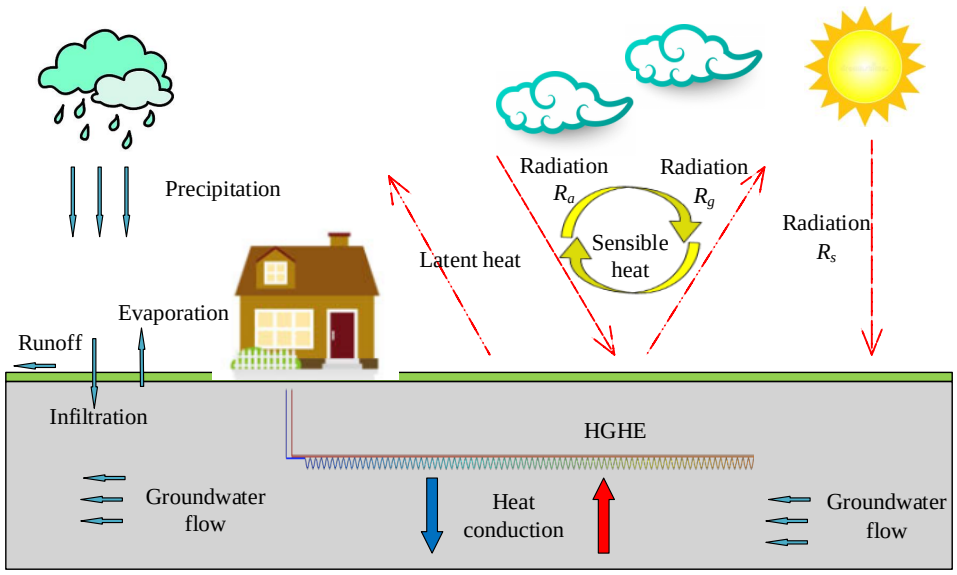


**Fig. 1**. Schematic of atmosphere-HGHE-ground interaction.

$$R_n = (1-a_l)R_s + R_a - R_g \tag{5}$$

where $a_l$ denotes the ground surface albedo and is set as 0.10 in this work (Tang and Nowamooz, 2020); $R_s$ represents the absorbed solar shortwave radiation, W/m$^2$; $R_a$ and $R_g$ are the atmospheric longwave radiation and outcoming ground surface longwave radiation, respectively, W/m$^2$. Besides:

$$R_a - R_g = \sigma\varepsilon\left(T_y^4 - T_s^4\right) \tag{6}$$

where $\sigma$ denotes Stephan-Boltzman constant, W/(m$^2$·K$^4$), and is equal to $5.67\times10^{-8}$ W/(m$^2$·K$^4$); $\varepsilon$ is the ground surface emissivity and is set as 0.97 (Tang and Nowamooz, 2020); $T_y$ represents the sky temperature, K, and is calculated by the cloud cover $C$ and air temperature $T_a$ (Cole, 1979). Here, the cloud cover $C$ is set as 0.82.

### 2.1.2 Fluid flow and heat transfer in GHE

The fluid flow and heat transfer processes in GHE are calculated by a 1-dimensional non-isothermal pipe flow model (Song et al., 2017; Shi et al., 2018), such as:

$$\frac{\partial(A\rho_f)}{\partial t} + \nabla\cdot(A\rho_f u_f) = 0 \tag{7}$$

$$\rho_f\frac{\partial u_f}{\partial t} = -\nabla p - \frac{1}{2}f_D\frac{\rho_f}{d}\mid u_f\mid u_f \tag{8}$$

$$\begin{aligned}&\rho_f A c_{p,f}\frac{\partial T}{\partial t} + \rho_f A c_{p,f}u_f\nabla T\\ &= \nabla\cdot\left(A\lambda_f\nabla T\right) + \frac{1}{2}f_D\frac{\rho_f A}{d}\mid u_f\mid u_f^2 + Q_w\end{aligned} \tag{9}$$

where $A$ denotes the cross section of the tube, m$^2$; $t$ denotes time, s; $\rho_f$ denotes the density of fluid, kg/m$^3$; $u_f$ denotes the velocity of fluid, m/s; $p$ denotes pore pressure, Pa; $f_D$ denotes Darcy friction factor to describe the viscosity shear, and is calculated by Churchill model (Churchill, 1977); $d$ denotes the hydraulic diameter of the pipe, m; $c_{p,f}$ denotes the heat capacity of the fluid, J/(kg·K); $T$ denotes temperature, K; $\lambda_f$ is the thermal conductivity of the fluid, W/(m·K); $Q_w$ represents the heat exchange between fluid and ground through pipe wall, W/m. Eqs. (7), (8) and (9) are respectively mass conservation equation, momentum equation and energy conservation equation in the pipe.

### 2.1.3 Ground fluid flow

Darcy's law is commonly used to describe the flow process in saturated soil. Meanwhile, the shallow soil is unsaturated because of the pores filled with air and water. Therefore, the unsaturated fluid flow process in shallow soil can be described by the Richards equation (Bear, 1972):

$$\rho_f C_m\frac{\partial p}{\partial t} + \nabla\cdot\left[-kk_r\nabla\cdot\rho_f(p+\rho_f g\nabla z)\right] = 0 \tag{10}$$

where $C_m$ denotes the specific water capacity, m$^{-1}$; $k$ and $k_r$ indicate the soil hydraulic conductivity and relative hydraulic conductivity, respectively, m/s; $\rho_f g\nabla z$ represents the gravity term; $g$ is acceleration of gravity and $z$ denotes the vertical direction. $k_r$ can be calculated by Mualem's equation (Mualem, 1976), such as:

$$k_r = \begin{cases} S_e^l\left[1-\left(1-S_e^{\frac{1}{m}}\right)^m\right]^2 & p<0\\ 1 & p\geq 0\end{cases} \tag{11}$$

where $l$ denotes the pore connectivity and is set as 0.5 here; $m$ is equal to $1-1/n$, where $n$ is the pore-size distribution; $S_e$ represents the effective saturation. The relationship between $S_e$ and suction can be described by the van Genuchten equation (Van Genuchten, 1980), such as:

$$k_r = \begin{cases} \left[1+\mid\alpha\frac{p}{\rho_f g}\mid^n\right]^{\frac{1}{n-1}} & p<0\\ 1 & p\geq 0\end{cases} \tag{12}$$

where $\alpha$ is related to the inverse of the air entry suction, m$^{-1}$.

### 2.1.4 Heat transfer in soil

The heat transfer process in soil can be given by (Song et al., 2018; Lin et al., 2021):

$$\rho_g c_{p,g}\frac{\partial T}{\partial t}+\rho_f c_{p,f} u_f \nabla T-\nabla\cdot(\lambda_g \nabla T)=-Q_w \tag{13}$$

where $\rho_g$ denotes the density of the soil, kg/m$^3$; $c_{p,g}$ denotes the heat capacity of the soil, J/(kg·K); $\lambda_g$ denotes the thermal conductivity of the soil, W/(m·K). The relationship between $c_{p,g}$, $\lambda_g$ and $S_r$ can be given by the following equations (Nikoosokhan et al., 2016; Tang and Nowamooz, 2020):

$$c_{p,g}=(4.18-0.3\chi_s-0.095\gamma_d)S_r-0.2\chi_s+0.09\gamma_d \tag{14}$$

$$\lambda_g=(0.443\chi_s+0.081\gamma_d)\frac{(4.4\chi_s+0.4)S_r}{1+(4.4\chi_s-0.6)S_r}+0.087\chi_s+0.019\gamma_d \tag{15}$$

where $S_r$ denotes the water saturation and is equal to $\theta/\theta_s$; $\chi_s$ and $\gamma_d$ denote sand content and dry unit weight of the soil, respectively, kN/m$^3$; $\theta$ is the volumetric water content, which can be obtained by:

$$\theta=\begin{cases}\theta_r+S_e(\theta_s-\theta_r) & p<0\\ \theta_s & p\geq 0\end{cases} \tag{16}$$

where $\theta_s$ and $\theta_r$ represent saturated water content and residual water content, respectively.

Since the wellbore in the GHE system is filled with backfill materials, the fluid flow and heat transfer processes are considered to be consistent with that in the soil and exhibit continuous boundary conditions.

## 2.2 Methodology

Fig. 2 shows the entire calculation process and method. Several major steps need to be performed to carry out this work. Firstly, a numerical model must be built, including the geometrical model, initial and boundary conditions, finite element meshes and setting of solver parameters. Then, the temperature field, thermal performances and economical efficiencies of the basic case are analyzed based on the constructed numerical model. Finally, the influences of two key factors on the thermal performances and economical efficiencies are studied.

The time step is set as 0.5 day for the first 10 days, 1 day for the next 20 days and 5 days for the rest of the time. The relative tolerance is considered as the convergence criteria of numerical solutions, and is set as $10^{-4}$.

## 2.3 Geometrical model and finite element mesh

The calculation region of the numerical model is 50 m depth, including soil, wellbore (backfill grout) and GHE. The soil and wellbore are 3-dimensional (3D) models, and the geometrical model of the GHE is simplified as a 1D model due to its small radius to reduce the workload. The soil is 28.5 m deep, and includes sand and clay. The density, thermal conductivity and heat capacity of the bedrock are equal to 2300 kg/m$^3$, 2.6 W/(m·K) and 0.9 J/(kg·K), respectively. The

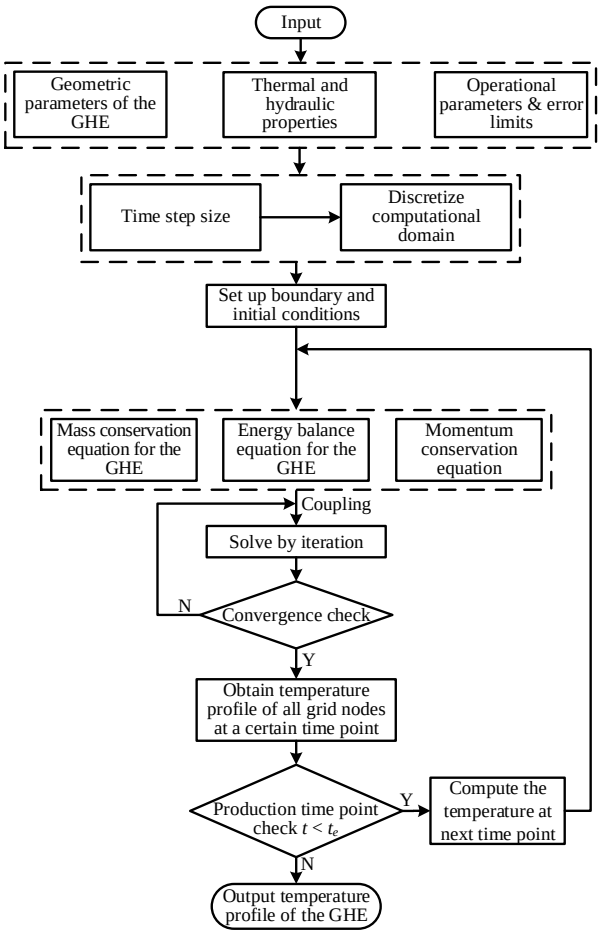


**Fig. 2**. The complete calculation process and method, where $t_e$ denotes the end time of simulation.

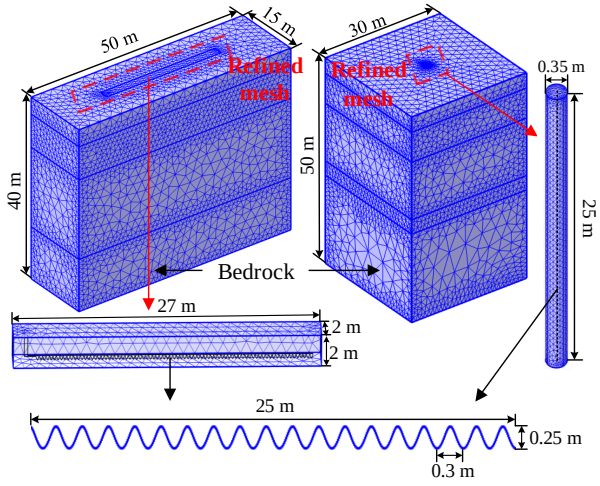


**Fig. 3**. Numerical meshing schemes.

circulating working fluid in GHE is water. The soil stratification and relevant parameters are shown in Table 1 (Tang and Nowamooz, 2019).

The computational domain of the HGHE is a rectangular block with a size of 50 m × 15 m × 40 m. The backfill grout is a cuboid with a size of 27 m × 2 m × 2 m (Congedo et

**Table 1**. Soil stratification and relevant parameters.

| Items | Depth (m) | $k$ (m/s) | $\alpha$ ($m^{-1}$) | $n$ (-) | $\theta_s$ (-) | $\theta_r$ (-) | $\chi_s$ (-) | $\rho_g$ (kg/m$^3$) | $\gamma_d$ (kN/m$^3$) |
|---|---|---|---|---|---|---|---|---|---|
| Sand | 3.7-11 | $1.03\times10^{-4}$ | 4.30 | 1.52 | 0.366 | 0.025 | 0.9 | 2540 | 16.1 |
| Clay | 0-3.7<br>11-28.5 | $1.44\times10^{-6}$ | 1.98 | 1.086 | 0.481 | 0.01 | 0.2 | 2740 | 14.2 |
| Backfill | - | $1.6\times10^{-9}$ | 0.02 | 1.52 | 0.20 | 0.01 | 0.62 | 2650 | 16 |

**Table 2**. Hydrothermal boundary conditions for the model.

| Surface | Hydraulic condition, value (unit) | Thermal condition, value (unit) |
|---|---|---|
| Top | Neumann, $W_i$ (mm/s) | Neumann, $G$ (W/m$^2$) |
| Lateral | No flow, - | Adiabatic, - |
| Bottom | Dirichlet, 0.343 (MPa) | Neumann, heat outflow (-) |

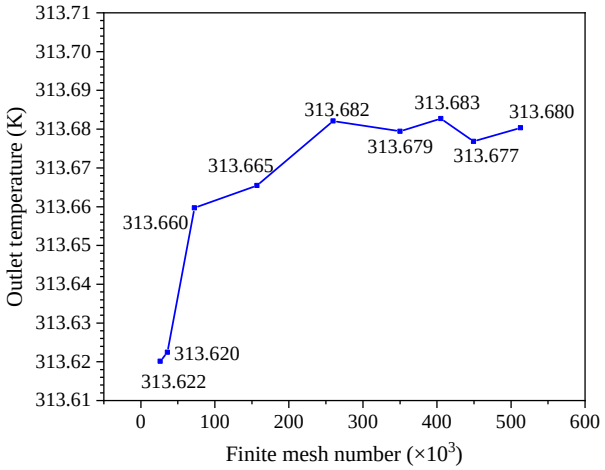


**Fig. 4**. Average outlet temperature in summer under different mesh numbers.

al., 2012) located in the center of the upper part of the soil cuboid. The length of the GHE is 25 m, and the tube is made from high-density polyethylene with 0.03 m inner diameter and 0.036 m outer diameter. The thermal conductivity of the tube is 0.5 W/(m·K). For the convenience of description, the sinusoidal function is used to characterize the shape of spiral tube. The computational domain of the VGHE is a rectangular block with a size of 30 m × 30 m × 50 m. The wellbore is a cylinder with a height of 25 m and a diameter of 0.35 m. The size of the VGHE is the same as that of the HGHE, and all other dimensions are detailed in Fig. 3.

The commercial finite element solver COMSOL is used to solve above partial differential equations. Fig. 3 depicts the meshing schemes of two models based on the free tetrahedral mesh method. Firstly, triangular meshes are generated at the top and bottom boundaries. Then, triangular meshes are generated on the remaining boundaries, and tetrahedral meshes are generated for the entire geometry. Finally, areas where different strata contact and the wellbore is located shall be refined for a better description of the temperature variation.

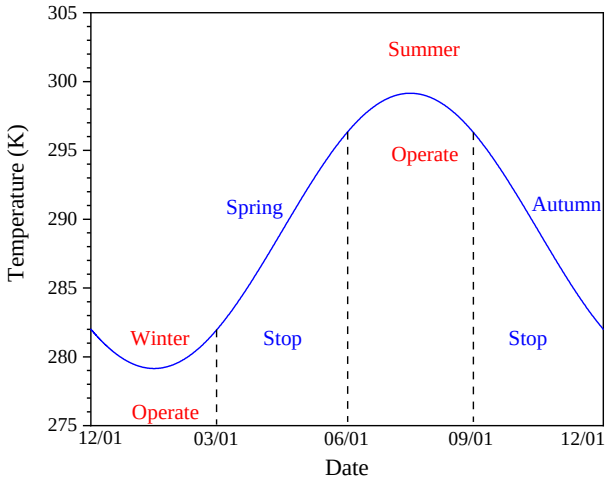


**Fig. 5**. Schematic of GHE operation scenario.

In order to minimize the error, the mesh thickness of the two models is basically set as identical, and the independence is verified by using the average outlet temperature in summer (Fig. 4). In view of the calculation accuracy and calculation time, the HGHE model is executed with a mesh quantity of 449295, and the VGHE model is executed with a mesh quantity of 368581.

## 2.4 Initial and boundary conditions

The investigated site is located in Chengdu, China. According to the data from the China Meteorological Administration, the average air temperature $T_a$, precipitation $P$ and shortwave radiation $R_s$ versus time are approximately cosine functions (Tang and Nowamooz, 2020; Shi et al., 2022), such as:

$$T_a = 289.15 + 10\cos\frac{2\pi(t + 137.5\times24\times3600)}{365\times24\times3600} \tag{17}$$

$$P = \frac{1}{30\times24\times3600} \times\left[115 + 110\cos\frac{2\pi(t + 137.5\times24\times3600)}{365\times24\times3600}\right] \tag{18}$$

$$R_s = 170 + 80\cos\frac{2\pi(t + 137.5\times24\times3600)}{365\times24\times3600} \tag{19}$$

The start time is the first day of winter. The ground heat exchanger operates only in summer and winter, and the schematic of the GHE operation scenario is shown in Fig. 5. The flow rate of working fluid is set as 0.3 kg/s. The inlet temperature of the GHE is set as 276.15 K in winter and 318.15 K in summer. The groundwater level remains constant at 5 m.

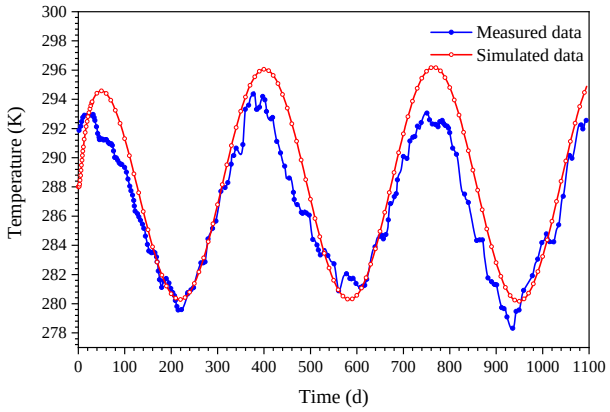


**Fig. 6**. Comparison between measured data and simulated data.

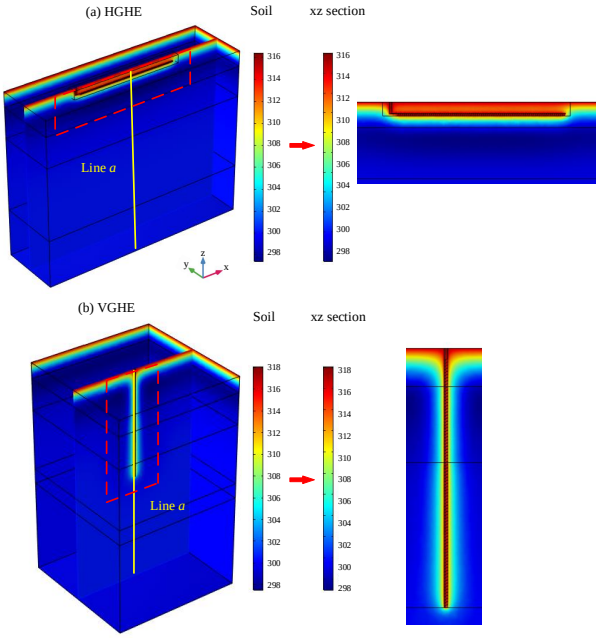


**Fig. 7**. Temperature contours in summer.

Herein, groundwater flow is not considered, and the top and bottom hydraulic boundaries are set as Neumann and Dirichlet conditions. The top hydraulic boundary is indicated by $W_i$ in Eq. (1), and the pressure on the bottom boundary stays constant at 0.343 MPa. No flow condition is imposed on the lateral boundaries. For the thermal boundary conditions, both the top and bottom boundaries are set as Neumann conditions. The top thermal boundary is $G$ in Eq. (3), and the bottom boundary is the heat outflow condition. The lateral boundaries are considered to be adiabatic. Table 2 summarizes all the imposed hydrothermal boundary conditions for this part.

The equilibrium method is used to acquire the initial conditions. In this way, the temperature and pressure of the original soil without the influence of GHE can be calculated, and temperature and pressure profiles are obtained, which are taken as the initial conditions.

### 2.5 Model validation

A 3D numerical model considering the effect of atmosphere and the variation of soil water content is built to simulate the fluid flow and heat transfer processes in the pipe of GHE and soil. In our previous works, the non-isothermal pipe flow model and the fluid flow and heat transfer coupling processes in the wellbore have been verified (Song et al., 2018; Shi et al., 2019a, 2019b). Therefore, the interaction model between atmosphere and soil will be verified in this section.

The measured data used to verify the accuracy of the model were collected by a temperature measuring device installed at 1.03 m below the ground surface in Alsace, France (Lin et al., 2020). The comparison between measured data and simulated data is shown in Fig. 6. It could be concluded that the root-mean-square error between the measured data and the simulation data was 2.18 K. Therefore, the numerical model can simulate the temperature variation of this area within a reasonable range.

## 3. Analysis of basic case

### 3.1 Temperature contours

Fig. 7 illustrates the temperature contours of HGHE and VGHE in summer (the 230$^{th}$ day). Fig. 8 shows the temperature distribution along line a (as shown in Fig. 7) at different times in winter and summer. According to the temperature distribution on the 45$^{th}$ day, as seen in Fig. 8, the soil temperature above the groundwater level changes greatly. As the depth increases, the soil temperature rises in winter and decreases in summer. The soil below the groundwater level is saturated, where the temperature is relatively stable because the soil thermal conductivity and heat capacity remain constant. In these areas, the relative hydraulic conductivity $k_r$ and water saturation $S_r$ remain constant at 1. Both in winter and summer, the soil temperature rises gradually with the increase in depth and tends to stabilize at 15 m below the ground surface. Besides, it can be seen from Figs. 7 and 8 that the temperature gradient near the GHE is the largest due to the heat extraction process, and the temperature near the ground surface alters greatly.

In winter, the soil temperature near the GHE decreases with time. The soil temperature alteration near the VGHE is about 22 °C compared with the original soil temperature, and there is a small difference in temperature between different time points. Besides, it can be seen that the soil temperature is distributed intermittently due to the presence of soil layers. The fluid temperature in the HGHE (as shown in Fig. 8) is generally slightly lower than that in the VGHE. The working fluid temperature is closer to the inlet temperature, and the soil temperature near the HGHE changes by about 16 °C compared with the original soil temperature. In addition, there are minor variations for the temperature below the HGHE at different time points, while the temperature above the HGHE shows obvious change.

In summer, the soil temperature near the GHE rises with time, changing by about 17 °C compared with the original soil temperature. The fluid temperature in the HGHE is slightly

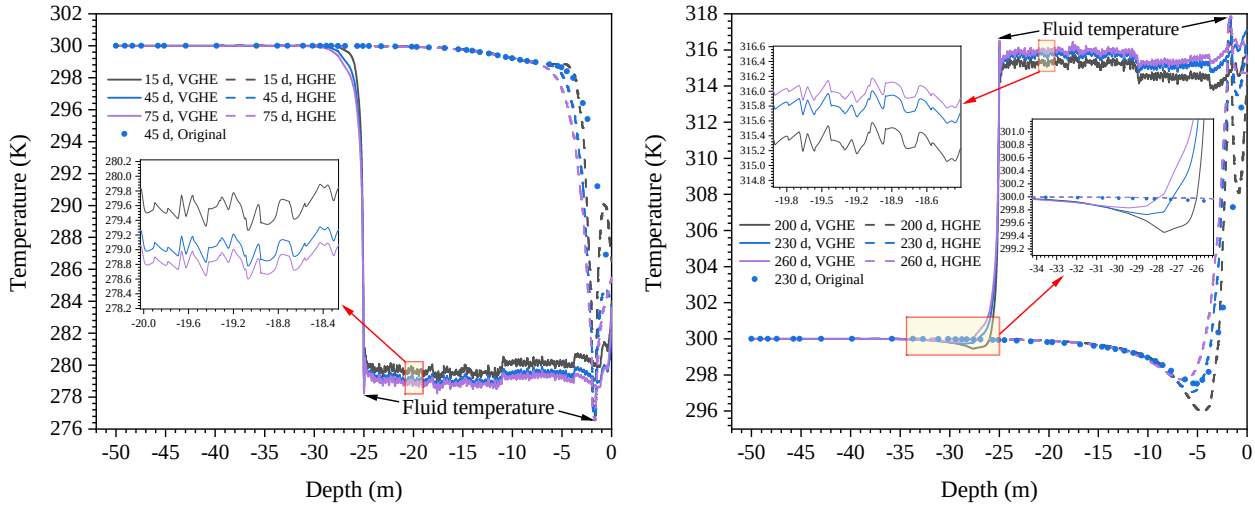


(a) Winter (b) Summer

**Fig. 8**. Temperature distributions along line a at different times in winter and summer.

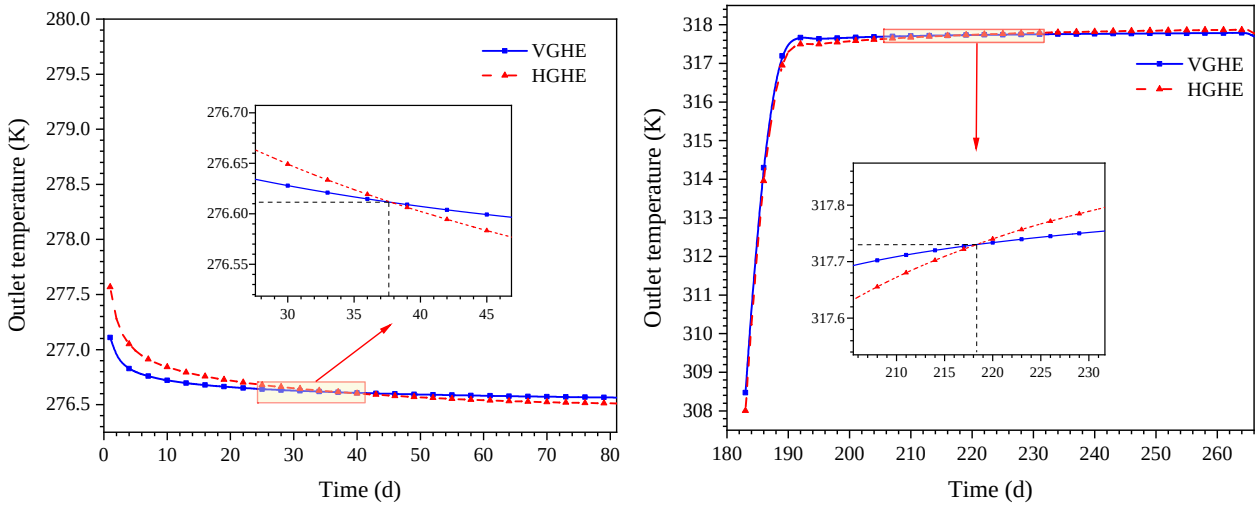


(a) Winter (b) Summer

**Fig. 9**. Outlet temperature of the two kinds of GHEs in winter and summer.

higher than that in the VGHE, which means that the effect of heat dissipation is relatively poor. The temperature near the HGHE changes by about 12 °C, whereas other features are similar to those in winter.

Furthermore, it can be observed that the variation amplitude of the temperature curve for the VGHE is much higher than that for the HGHE. This is because for the VGHE, the area that line *a* passes through is the soil in the central part of the spiral tube, and there will be a fluctuation as soon as it passes through a circle of the spiral tube.

## 3.2 Outlet temperature and thermal power

The inlet temperatures of the two kinds of GHEs in winter and summer are 3 and 45 °C, respectively. According to Fig. 9, except for the abrupt section at the beginning of fluid injection, the outlet temperature of the VGHE remains stable in winter, while the initial outlet temperature of the HGHE is higher, and then it decreases significantly. The heat exchange efficiency becomes gradually worse, but the overall variation is small. On the 38$^{th}$ day, the outlet temperatures of the two GHEs are the same. The outlet temperature alteration of the VGHE is also minor in summer. The initial outlet temperature of the HGHE is lower than that of the VGHE, and then it increases significantly. The efficiency of heat exchange becomes gradually lower, but the overall change is small. On the 218$^{th}$ day, the outlet temperatures of the two GHEs are the same.

The reason for the above phenomenon is mainly related to the installation direction of the two kinds of GHEs. The VGHE is installed along the vertical direction, which is less affected by surface radiation and precipitation. The soil temperature around the heat exchanger is stable, and the outlet temperature

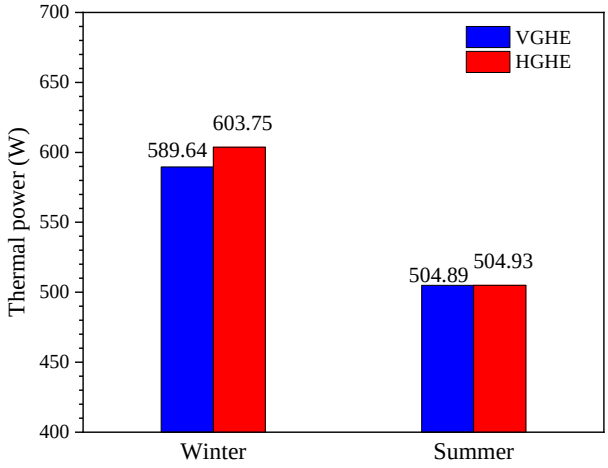


**Fig. 10**. Thermal power of the two heat exchangers in winter and summer.

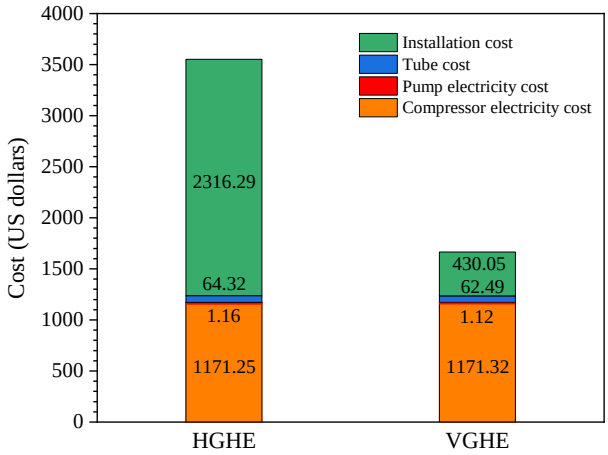


**Fig. 11**. Comparison of total cost for the basic case.

is relatively constant. However, due to the long-term heat exchange process, the temperature difference between the heat exchanger and soil becomes smaller, and the outlet temperature gradually approaches the inlet temperature. Meanwhile, the HGHE is installed in the horizontal direction, and the whole heat exchanger is located in the backfill grout within 2 m below the ground surface. The soil temperature changes greatly, and the temperature difference between the HGHE and soil is slightly larger than that in the VGHE. Therefore, the heat exchange capacity is better in the early stage. Due to the air temperature variation and the development of heat exchange process, however, the temperature difference between HGHE and soil decreases rapidly. The heat exchange capacity gradually declines, and the amplitude is greater than that in the VGHE. This can be verified by Fig. 8.

In order to facilitate the expression, the thermal power is expressed by the average thermal power during the total operation periods, which can be calculated by:

$$P_w = \frac{\int_t q_c c_{p,f(T_o-T_i)}}{\Delta t_w} \tag{20}$$

$$P_s = \frac{\int_t q_c c_{p,f(T_i-T_o)}}{\Delta t_s} \tag{21}$$

where $P_w$ and $P_s$ respectively denote the average thermal power in winter and summer; $q_c$ denotes the circulation mass flow rate in the heat exchanger, kg/s; $T_i$ and $T_o$ respectively represent the inlet and outlet temperatures of the heat exchanger, K; $\Delta t_w$ and $\Delta t_s$ respectively represent operation time in winter and summer.

The thermal power of the two heat exchangers in winter is higher than that in summer (Fig. 10), indicating that their heat exchange efficiency is better in winter. Moreover, the thermal power of the HGHE is about 14 W higher than that of the VGHE in winter, but there is a small difference between them in summer. This is because the soil temperature variation caused by GHEs in winter is larger than that in summer, resulting in a large difference between the outlet temperature and inlet temperature. Besides, the ambient temperature difference between VGHE and HGHE is minor due to their short lengths. Therefore, although the heat exchange efficiency of the HGHE decreases rapidly over time, its thermal power is greater than that of the VGHE.

## 3.3 Economic efficiency

Economic efficiency here denotes the total cost comparison of the two heat exchangers, including installation cost, tube cost and operation cost (Kayaci and Demir, 2020). The installation cost consists of drilling cost and backfilling cost. The backfill material price is \$13.73/m$^3$ (Sun and Li, 2013) and the unit tube price is \$0.67/m. The operation cost includes the electricity cost of the circulating pump $E_p$ and the electricity cost of the heat pump compressor $E_c$, which can be calculated by:

$$E_p = \frac{(\Delta t_w + \Delta t_s) q_c p_i}{\eta} C_e \tag{22}$$

$$E_c = \left( \frac{Q_h}{\mathrm{COP}_h} \Delta t_w + \frac{Q_c}{\mathrm{COP}_c} \Delta t_s \right) C_e \tag{23}$$

where $p_i$ denotes the pump injection pressure, Pa; $\eta$ denotes the pump efficiency and is set as 0.7 here; $C_e$ denotes the unit cost of electricity, \$/(kW·h), and it always remains \$0.077/(kW·h); $Q_h$ and $Q_c$ represent the heating and cooling thermal power required by the building, respectively, W; $\mathrm{COP}_h$ and $\mathrm{COP}_c$ respectively represent the heating coefficient and cooling coefficient of the performance; The building area is assumed to be 100 m$^2$ in size. $Q_h$ and $Q_c$ are 15000 W and 11500 W, respectively. $\mathrm{COP}_h$ and $\mathrm{COP}_c$ can be determined by the following formulas (Hein et al., 2016):

$$\mathrm{COP}_h = 0.083 T_o + 3.925 \tag{24}$$

$$\mathrm{COP}_c = -0.12 T_o + 8.6 \tag{25}$$

where the space heating and cooling temperature are set as 35 and 18 °C, respectively.

Due to the huge difference in the installation cost, the total cost of the HGHE is much higher than that of the VGHE (Fig. 11). This is because a larger space and more backfill materials

are required to install the HGHE, while the drilling cost of the VGHE is not high in shallow soil and the backfill volume is smaller. In addition, in this study, we tried to compare two kinds of heat exchangers with the same structure and length, and the tube costs are slightly different due to the different installation direction. Furthermore, due to the small difference between the outlet temperature and the inlet pressure, the electricity costs of two heat exchangers are relatively close to each other.

The conclusion on the installation cost is different from the traditional cognition, which is specifically explained here. It is assumed that the soil in the study is clay. The reference standards for the installation cost are shown in Table 3 (Qi, 2018). The installation cost ratio of the horizontal and vertical ground heat exchangers can be calculated as:

$$\frac{C_h}{C_v} = \frac{(C_1 + C_b)S_{c,h}l_h}{C_2 l_v + C_b S_{c,v} l_v} \tag{26}$$

where $C_h$ and $C_v$ respectively denote the installation cost of the HGHE and VGHE, \$; $C_1$ and $C_2$ are respectively the unit installation price of HGHE and VGHE, \$; $C_b$ denotes the backfill material price, \$/m$^3$, and it is set as \$13.73/m$^3$ here; $l_h$ and $l_v$ respectively represent the length of backfill grout and wellbore, m; $S_{c,h}$ and $S_{c,v}$ respectively denote the sectional area of backfill grout and wellbore, m$^2$. $S_{c,h}$ and $S_{c,v}$ are equal to 4 m$^2$ and 0.096 m$^2$, respectively (as shown in Fig. 3). The tube volume is not considered here due to the small diameter.

As can be seen from Table 3, the unit price difference between drilling and trial trench is minor for a short length. To simplify the calculation process, it is assumed that the length of the backfill grout and wellbore are the same. $C_1$ and $C_2$ are \$7.72 and \$15.44, respectively. It is found that the installation cost of the HGHE (including the backfilling cost) is about 5 times of that of the VGHE.

**Table 3**. Unit price list for the physical work of geotechnical engineering exploration (Qi, 2018).

| Items | D[a] | Price |
|---|---|---|
| Drilling[b] | D ≤ 10 m | \$10.54/m |
| | 10 m < D ≤ 20 m | \$13.21/m |
| | 20 m < D ≤ 30 m | \$15.88/m |
| | 30 m < D ≤ 40 m | \$18.85/m |
| | 40 m < D ≤ 50 m | \$22.41/m |
| | 50 m < D ≤ 60 m | \$24.94/m |
| | 60 m < D ≤ 80 m | \$27.76/m |
| | 80 m < D ≤ 100 m | \$30.28/m |
| Trial trench | D ≤ 2 m | \$7.72/m$^3$ |
| | D > 2 m | \$11.13/m$^3$ |

Notes: [a]D denotes the depth; [b]In drilling, multiply the base price of the previous gear by 1.3 for every 20 m increase when D >100 m.

## 4. Effects of injection mass flow rate

In the previous section, it has been demonstrated that the outlet temperature has an important impact on the thermal power and the heat pump compressor electricity cost, while the injection mass flow rate has a great influence on the circulation pump electricity cost. Thus, this section compares the thermal performances and economical efficiencies under different injection mass flow rates.

### 4.1 Outlet temperature

Fig. 12 plots the outlet temperature of the two GHEs against time under different injection mass flow rates in winter and summer. The outlet temperature curve is similar to that for the basic case. In winter, the outlet temperature decreases with the increase of injection mass flow rate, and the amplitude becomes smaller. In summer, the outlet temperature rises with the increase of injection mass flow rate, and the increase amplitude also decreases. This is because the increment of the injection mass flow rate shortens the heat exchange time between working fluid and soil, making the average outlet temperature approach the inlet temperature.

In addition, the outlet temperature curves of different injection mass flow rates will intersect at the same time point, and then stabilize on the last day of the operation period. The influence of injection mass flow rate is more obvious on the outlet temperature of the HGHE than the VGHE; however, the amplitude decreases with the inlet flow rate increment. These two curves basically coincide when the injection mass flow rate reaches 0.0006 m$^3$/s.

This is because when the inlet flow rate is low, the HGHE is affected by surface radiation and precipitation for a longer period, and the heat exchange is more sufficient compared with the VGHE. The influence time of surface radiation and precipitation is shortened and their functions are greatly reduced by increasing the inlet flow rate. Besides, it can be found that when the flow rate is low, the outlet temperature difference between the two GHEs is large, and increasing the flow rate will weaken this difference.

### 4.2 Economic efficiency

Since the injection mass flow rate does not affect the tube cost and installation cost, the operation cost of the two heat exchangers is mainly considered in this section, including the electricity costs of heat pump compressor and circulation pump. As indicated in Fig. 14, it can be found that in addition to the tube cost and installation cost, the electricity cost of heat pump compressor is an important component of the operation cost.

### 4.3 Thermal power

In winter, the thermal power of both heat exchangers increases linearly with the rise of injection mass flow rate. The thermal power of the HGHE is higher than that of the VGHE, with a difference of about 14 W. In summer, the thermal power is stable when the injection mass flow rate changes, and the difference between two heat exchangers is very small. It can be found that increasing the injection mass flow rate is beneficial

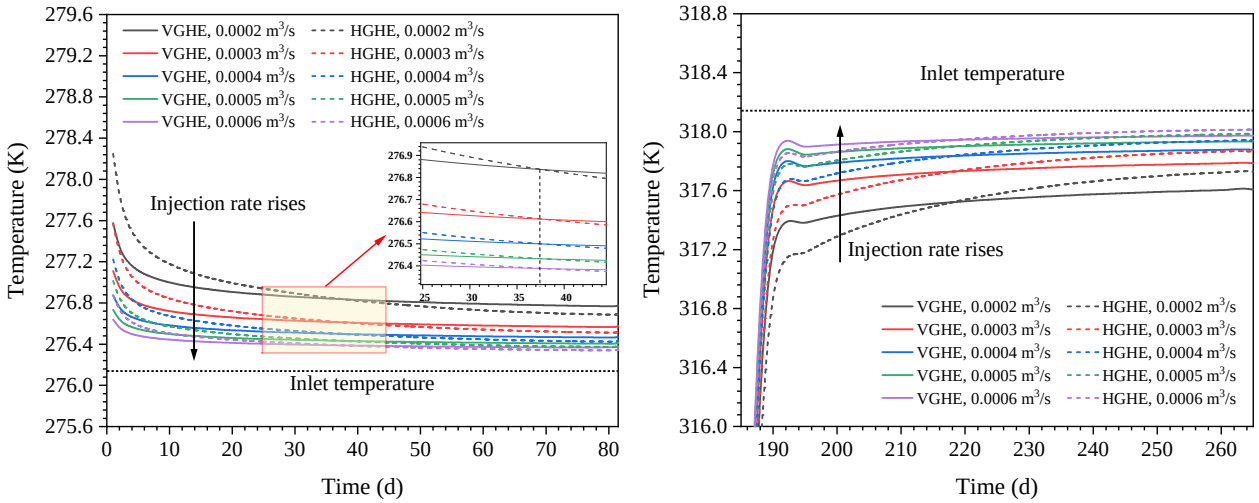


(a) Winter (b) Summer

**Fig. 12**. Outlet temperature of the two kinds of GHE with time under different injection mass flow rates.

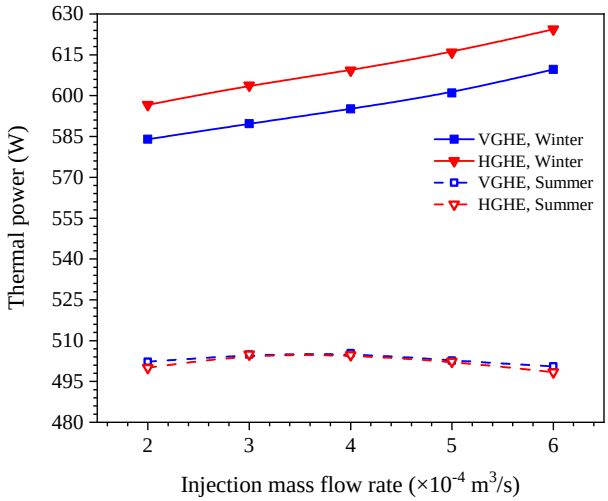


**Fig. 13**. Comparison of thermal power between the two heat exchangers under different injection mass flow rates.

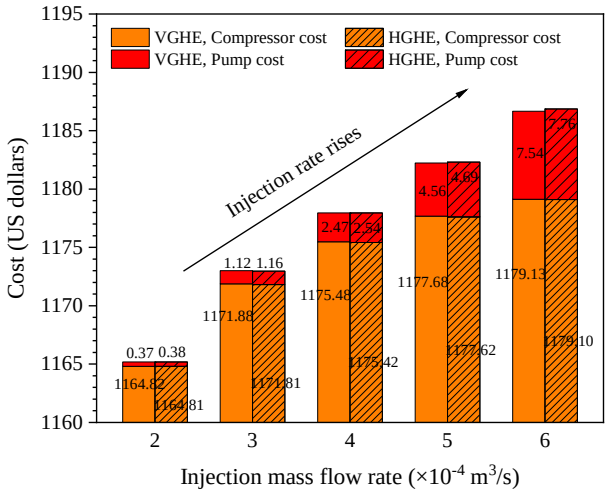


**Fig. 14**. Cost comparison under different injection mass flow rates.

for the heat extraction in winter, but it has a smaller effect on heat dissipation in summer. In general, the injection mass flow rate has a minor effect on the thermal power.

The increase in injection mass flow rate leads to the obvious increase in the heat pump compressor electricity cost and circulation pump electricity cost. A smaller rate has a greater impact on the electricity cost of heat pump compressor, and a larger rate has a greater impact on the electricity cost of circulation pump. Generally speaking, the differences in operation costs between the two heat exchangers are negligible. Therefore, the injection mass flow rate has a minor effect on the economic difference between vertical and horizontal ground heat exchangers, and the rise in the injection mass flow rate can increase the cost.

## 5. Effects of GHE length

From the previous section, it can be concluded that the total cost mainly comprises the installation cost, and the length has a greater impact on the VGHE. Therefore, this section compares the thermal performances and economical efficiencies under different GHE lengths.

### 5.1 Outlet temperature

The outlet temperatures of the HGHE and VGHE rise linearly with the increase in heat exchanger length in winter and they decrease in summer (Fig. 15). This is because a long heat exchange tube is able to enhance the heat exchange.

In addition, with the increase in length, the variation trend of outlet temperature with time is similar to that in the previous section, whereas the outlet temperature difference between two GHEs becomes larger. This shows that with the increase in length, the outlet temperature of the HGHE rapidly approaches the inlet temperature, and the heat exchange efficiency becomes worse compared with the VGHE. This is because the area affected by the surface radiation and precipitation increases, resulting in a dramatic change in outlet temperature.

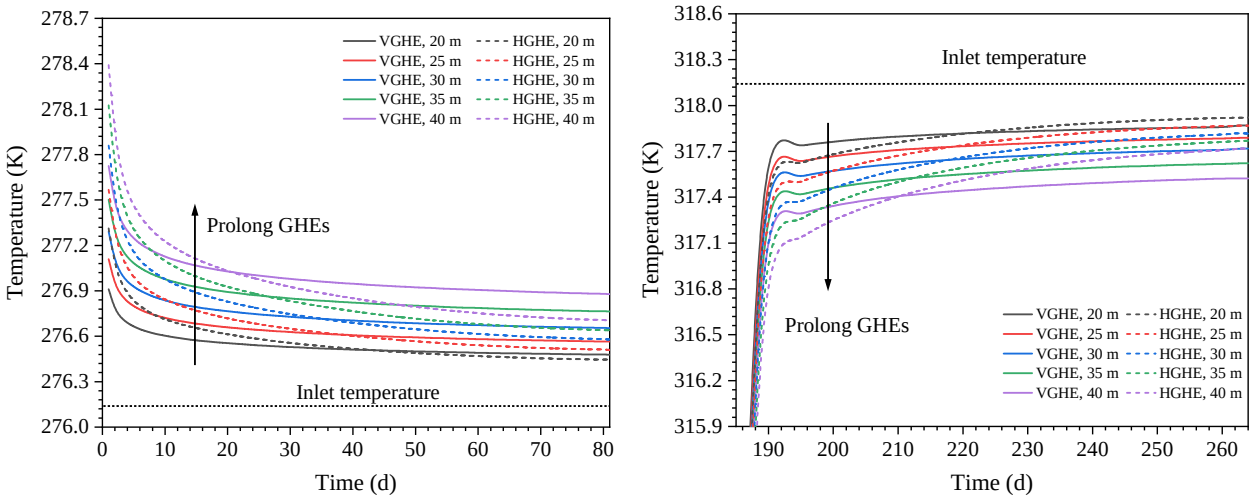


(a) Winter (b) Summer

**Fig. 15**. Outlet temperature under different heat exchanger lengths in winter and summer.

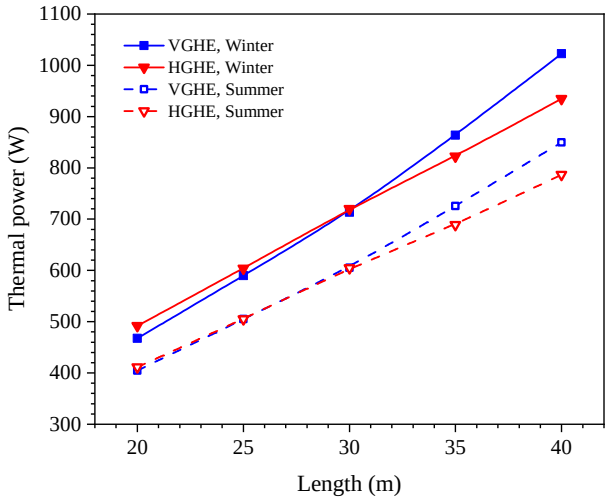


**Fig. 16**. Thermal power comparison under different GHE lengths.

### 5.2 Thermal power

Fig. 16 presents the comparison of thermal power under different GHE lengths. It can be seen that with the increase in length, the thermal power of the two heat exchangers increases both in winter and in summer. The thermal power of the HGHE is higher when the length is less than 30 m, and the thermal power of the VGHE is higher when the length is more than 30 m. As the length increases, the difference between the two GHEs rises, which is consistent with the results obtained in Fig. 15. Therefore, the length of GHE has a greater impact than the injection mass flow rate (especially on the VGHE).

### 5.3 Economic efficiency

As shown in Fig. 17, the total cost of the two heat exchangers rises with the increase in their length, and it mainly constitutes the electricity cost of heat pump compressor for the VGHE and mainly the installation cost for the HGHE. With the increase in length, apart from the negligible reduction of heat pump compressor electricity cost, all of the circulation pump electricity cost, tube cost and installation cost show a rising trend. Besides, the total cost of the HGHE (essentially the installation cost) is much higher than that of the VGHE for the same length. Therefore, the thermal performances and installation costs (especially the price of backfill materials) should be paid attention to when installing ground heat exchangers in shallow soil.

## 6. Conclusions

In this work, the thermal performances and economical efficiencies of shallow vertical and horizontal ground heat exchangers with the same structure and length were compared using a 3D numerical model, which considers the changes of surface environment and underground water content. The atmosphere-HGHE-soil interaction and temperature contours between two kinds of shallow heat exchangers were analyzed. The thermal performances and economical efficiencies were compared between winter and summer, and the effects of injection mass flow rate and GHE length were studied. The study site is located in Chengdu, China, with an average temperature in winter of about 7 °C, and an average monthly precipitation of about 18 mm. These parameters in summer are about 25 °C and about 212 mm, respectively. Based on the above climatic conditions, some key findings of this study could be established as follows:

- The outlet temperature of the VGHE is relatively stable, but it is easily affected by soil layers. The ambient temperature of the HGHE exhibits significant changes, and the temperature difference between inlet and outlet decreases rapidly over time. Besides, compared with the summer, the thermal performance difference between VGHE and HGHE is larger in winter.
- The thermal performance of the two heat exchangers is

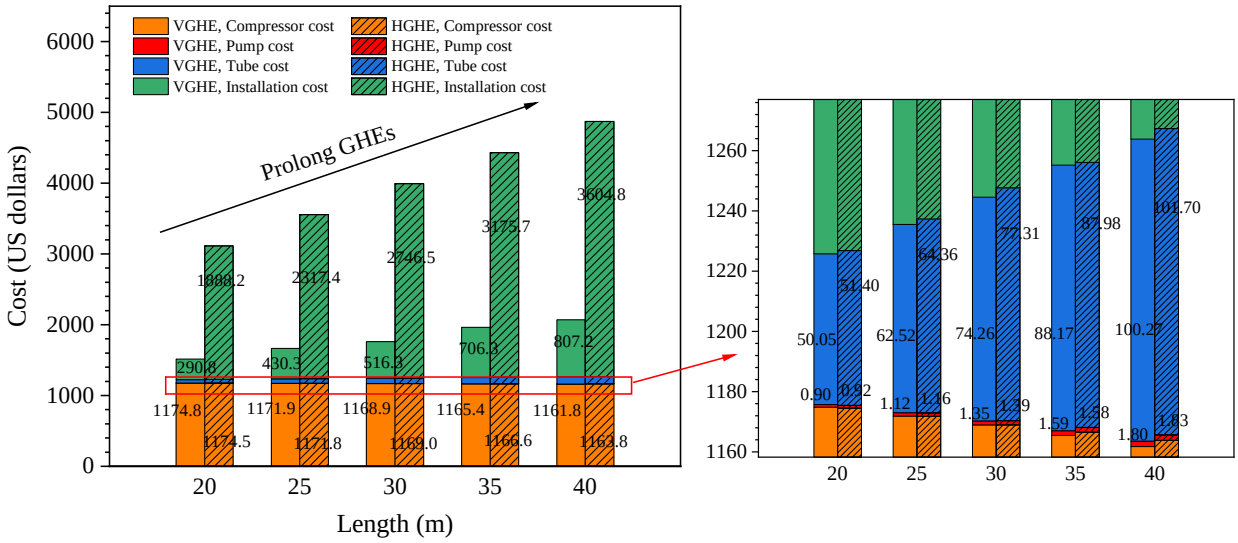


**Fig. 17**. Cost comparison under different GHE lengths.

hardly influenced by the injection mass flow rate, while it is significant impacted by the GHE length. Whether in winter or summer, the thermal performance of two heat exchangers rises linearly with the increase in their length, and the VGHE is more sensitive in this respect. Under the conditions set in the present paper, the thermal power of a spiral VGHE is higher than that of a spiral HGHE when the length of the heat exchanger is more than 30 m.

- Based on the calculation of economical efficiencies, the total cost of a HGHE is much higher than that of a VGHE within the range of GHE length considered in this paper. This is because the installation cost of the HGHE is much higher than that of the VGHE, while the heat pump compressor electricity cost and other costs are relatively similar.
- In view of the observed thermal performances and economical efficiencies, a VGHE is recommended when installing a single shallow ground heat exchanger. In addition, due to the smaller required construction area of ground facilities and backfilling workload, the VGHE system has a smaller space demand.
- The results for thermal performance and economic efficiency were obtained under an atmospheric condition. Due to the significant influences of atmospheric conditions, the thermal performances in different regions may vary, which is an important aspect to consider in our future research. However, the results on economical efficiencies can be used as a reference for relevant research in other regions.

## Acknowledgements

The authors would like to acknowledge the support of the Sichuan Science and Technology Program (No. 2021YJ0389). Besides, all support from the National Natural Science Foundation of China (No. 52104034), Foundation of State Key Laboratory of Petroleum Resources and Prospecting, China University of Petroleum, Beijing (No. PRP/open-2110) and the Fundamental Research Funds for the Central Universities (No. 2682021CX059) is highly appreciated.

## Conflict of interest

The authors declare that they have no known competing financial interests or personal relationships that could have appeared to influence the work reported in this paper.



## References

Bear, J. Dynamics of Fluids in Porous Media. New York, USA, Elsevier Scientific Publishing, 1972.

Chalhoub, M., Bernier, M., Coquet, Y., et al. A simple heat and moisture transfer model to predict ground temperature for shallow ground heat exchangers. Renewable Energy, 2017, 103: 295-307.

Chen, X., Buchberger, S. G. Exploring the relationships between warm-season precipitation, potential evaporation, and "apparent" potential evaporation at site scale. Hydrology and Earth System Sciences, 2018, 22(8): 4535-4545.

Chen, S., Ding, B., Gong, L., et al. Comparison of multi-field coupling numerical simulation in hot dry rock thermal exploitation of enhanced geothermal systems. Advances in Geo-Energy Research, 2019, 3(4): 396-409.

Choi, W., Ooka, R., Nam, Y. Impact of long-term operation of ground-source heat pump on subsurface thermal state in urban areas. Sustainable Cities and Society, 2018, 38: 429-439.

Churchill, S. W. Friction-factor equation spans all fluid-flow regimes. Chemical Engineering Journal, 1977, 84: 91-92.

Cole, R. J. The longwave radiation incident upon inclined surfaces. Solar Energy, 1979, 22(5): 459-462.

Congedo, P. M., Colangelo, G., Starace, G. CFD simulations of horizontal ground heat exchangers: A comparison among different configurations. Applied Thermal Engineering, 2012, 33: 24-32.

Dada, M., Benchatti, A. Assessment of heat recovery and recovery efficiency of a seasonal thermal energy storage system in a moist porous medium. International Journal of Heat and Technology, 2016, 34(4): 701-708.

Dietrich, O., Fahle, M., Seyfarth, M. Behavior of water balance components at sites with shallow groundwater tables: Possibilities and limitations of their simulation using different ways to control weighable groundwater lysimeters. Agricultural Water Management, 2016, 163: 75-89.

Gosselin, J. S., Raymond, J., Gonthier, S., et al. Nanocomposite materials used for ground heat exchanger pipes. Paper Presented at IGSHPA Technical/Research Conference and Expo 2017, Denver, Colorado, 14-16 March, 2017.

Habibi, M., Hakkaki-Fard, A. Evaluation and improvement of the thermal performance of different types of horizontal ground heat exchangers based on techno-economic analysis. Energy Conversion and Management, 2018, 171: 1177-1192.

Hein, P., Kolditz, O., Görke, U. J., et al. A numerical study on the sustainability and efficiency of borehole heat exchanger coupled ground source heat pump systems. Applied Thermal Engineering, 2016, 100: 421-433.

Javadi, H., Ajarostaghi, S. S. M., Pourfallah, M., et al. Performance analysis of helical ground heat exchangers with different configurations. Applied Thermal Engineering, 2019, 154: 24-36.

Kayaci, N., Demir, H. Comparative performance analysis of building foundation ground heat exchanger. Geothermics, 2020, 83: 101710.

Kazemi, H., Ehyaei, M. A. Energy, exergy, and economic analysis of a geothermal power plant. Advances in Geo-Energy Research, 2018, 2(2): 190-209.

Kim, M. J., Lee, S. R., Yoon, S., et al. Evaluation of geometric factors influencing thermal performance of horizontal spiral-coil ground heat exchangers. Applied Thermal Engineering, 2018, 144: 788-796.

Kong, X. R., Deng, Y., Li, L., et al. Experimental and numerical study on the thermal performance of ground source heat pump with a set of designed buried pipes. Applied Thermal Engineering, 2017, 114: 110-117.

Lin, J., Nowamooz, H., Braymand, S., et al. Impact of soil moisture on the long-term energy performance of an earth-air heat exchanger system. Renewable Energy, 2020, 147: 2676-2687.

Lin, Z., Liu, K., Liu, J., et al. Numerical model for geothermal energy utilization from double pipe heat exchanger in abandoned oil wells. Advances in Geo-Energy Research, 2021, 5(2): 212-221.

Monteith, J. L. Evaporation and environment. Symposia of the Society for Experimental Biology, 1965, 19: 205-234.

Mualem, Y. A new model for predicting the hydraulic conductivity of unsaturated porous media. Water Resources Research, 1976, 12(3): 513-522.

Muther, T., Syed, F. I., Lancaster, A. T., et al. Geothermal 4.0: AI-enabled geothermal reservoir development-current status, potentials, limitations, and ways forward. Geothermics, 2022, 100: 102348.

Nikoosokhan, S., Nowamooz, H., Chazallon, C. Effect of dry density, soil texture and time-spatial variable water content on the soil thermal conductivity. Geomechanics and Geoengineering, 2016, 11(2): 149-158.

Pu, L., Xu, L., Qi, D., et al. Structure optimization for horizontal ground heat exchanger. Applied Thermal Engineering, 2018, 136: 131-140.

Qi, L. Application manual of charge standard for engineering investigation and design. Beijing, China Market Publishing House, 2018. (in Chinese)

Shi, Y., Cui, Q., Song, X., et al. Study on thermal performances of a horizontal ground heat exchanger geothermal system with different configurations and arrangements. Renewable Energy, 2022, 193: 448-463.

Shi, Y., Song, X., Li, G., et al. Numerical investigation on heat extraction performance of a downhole heat exchanger geothermal system. Applied Thermal Engineering, 2018, 134: 513-526.

Shi, Y., Song, X., Wang, G., et al. Numerical study on heat extraction performance of a multilateral-well enhanced geothermal system considering complex hydraulic and natural fractures. Renewable Energy, 2019a, 141: 950-963.

Shi, Y., Song, X., Wang, G., et al. Study on wellbore fluid flow and heat transfer of a multilateral-well $CO_2$ enhanced geothermal system. Applied Energy, 2019b, 249: 14-27.

Song, X., Shi, Y., Li, G., et al. Numerical simulation of heat extraction performance in enhanced geothermal system with multilateral wells. Applied Energy, 2018, 218: 325-337.

Song, X., Shi, Y., Li, G., et al. Heat extraction performance simulation for various configurations of a downhole heat exchanger geothermal system. Energy, 2017, 141: 1489-1503.

Sun, D., Li, Q. Analysis on the performance-price ratio of the backfill of ground source heat pump in Tai'an area. Technology Innovation and Application, 2013, 36: 10. (in Chinese)

Tang, F., Nowamooz, H. Factors influencing the performance of shallow borehole heat exchanger. Energy Conversion and Management, 2019, 181: 571-583.

Tang, F., Nowamooz, H. Outlet temperatures of a slinky-type horizontal ground heat exchanger with the atmosphere-soil interaction. Renewable Energy, 2020, 146: 705-718.

Van Genuchten, M. T. A closed-form equation for predicting the hydraulic conductivity of unsaturated soils. Soil Science Society of America Journal, 1980, 44(5): 892-898.

Yang, P., Xu, R., Wang, F., et al. Numerical simulation and experimental validation on the heat transfer characteristics of horizontal spiral coil ground heat exchanger. Journal of Engineering Thermophysics, 2021, 42(8): 2122-2131. (in Chinese)

Zhang, X., Hu, Q. Development of geothermal resources in China: A review. Journal of Earth Science, 2018, 29(2): 452-467.